A multimodal metabolomics approach to elucidate the trigger components of rumen fluid for larval exsheathment in a model gastrointestinal parasitic nematode, *Haemonchus contortus*.

Nikola Palevich[1*], Paul H. Maclean[1], Arvind K. Subbaraj[2] and Mingshu Cao[1].

[1]AgResearch Ltd., Grasslands Research Centre, Palmerston North, 4442, New Zealand.

[2]AgResearch Ltd., Lincoln Research Centre, Christchurch, 8140, New Zealand.

*Corresponding author: E-mail: nik.palevich@agresearch.co.nz

Keywords

Haemonchus contortus, metabolomics, lipidomics, helminth, parasite, rumen, exsheathment.

Abstract

In nematodes that invade the gastro-intestinal tract of the ruminant, the process of larval exsheathment marks the transition from the free-living to the parasitic stages of these parasites. To investigate larval exsheathment, a closed *in vitro* system that effectively reproduces the two basic components of an anaerobic rumen environment (CO_2 and 39 °C) was developed to trigger exsheathment in one of the most pathogenic and model gastrointestinal parasitic nematode, *Haemonchus contortus* (barber‘s pole worm). This project applied the basic principles of dialysis and is the first reported use of all currently available non-specific metabolomics methodologies to identify the rumen-derived trigger compounds associated with larval development in *H. contortus*. Herein, we report an multimodal untargeted metabolomics and lipidomics analyses based on 20 kDa (n = 10), 8-10 kDa (n = 10) and 100 Da (n = 10) molecular weight cut-off dialyzed rumen fluid fractions, all of which demonstrated positive

effects on exsheathment induction *in vitro* under rumen conditions, as compared to control infective third-stage larva (L3) in saline (n = 10). Metabolite identification and multivariate analyses resulted in a catalogue of over one thousand structurally annotated compounds or metabolites that form three distinct cluster groups and warrant further investigation. The multimodal metabolomics analyses revealed significant alterations between the three different rumen fluid fractions in L-lactic acid, pyruvate metabolism, gluconeogenesis, the Warburg effect, plant-pathogen interaction, plant hormone signal transduction, and biosynthesis of amino acids metabolism. Lysophosphatidylglycerol, diglyceride, phosphatidylcholine, triglyceride and a sterol were the major lipid classes identified by the non-targeted lipidomics method applied. A combination of univariate and multivariate statistical analyses revealed a panel of metabolites directly responsible for larval exsheathment and associated with amino acids as well as purine and pyruvate metabolism KEGG pathways. Among these were compounds such as methionine, leucine, alanine, phenylalanine, xanthine and hypoxanthine, that were significant in the control group and identified using two separate metabolomics streams. This study presents an *in vitro* system suitable for numerous functional omics' experimentation applications and has enhanced our understanding of the distinct molecular and metabolic pathways associated with larval exsheathment. The identified metabolites may serve as metabolic signatures or novel metabolic biomarkers for pre-diagnostic purposes of haemonchosis. Alternatively, our findings can be used to develop next-generation biomimicry agents to cause infective larvae of parasitic nematodes to exsheath outside the host while on pasture for experimental or control purposes.

Introduction

Parasitic nematodes cause numerous diseases with major consequences to the most disadvantaged human communities and agricultural production (1, 2). From an agricultural perspective, *Haemonchus contortus* (barber's pole worm), is one of the most economically important internal pathogenic nematodes infecting small ruminants, such as sheep and goats, and is a global animal health issue causing drastic losses in livestock (3). These blood-feeding strongylid nematodes are orally transmitted via contaminated pasture to the host where they penetrate the fourth stomach (abomasum) mucosa causing anemia and associated complications, often leading to death (4). Although many worm species can be managed using existing prophylactic drugs (anthelmintics), research in this space is important owing to their remarkable natural tendency to develop resistance combined with the excessive use and consequent diminishing efficacy demonstrated for both old and new chemicals, threatens the global livestock industry (5-7).

In nematodes that invade the gastro-intestinal tract of the ruminant, ecdysis (εκδυο, ekduo, ''to take or strip off''), is a key developmental process involving the moulting of the cuticle (8). In *H. contortus* and related nematodes, the post-embryonic stages of the life cycle are marked by four sequential moults, where larval exsheathment does not take place until the infective third-stage larva (L3) enters the rumen (9-11). This sheath provides protection from various external environmental stresses such as low temperatures and desiccation (12). The L3s emerge from within their sheath (xL3) once they are exposed to the drastic rumen conditions, namely an increase in temperature (39°C), a strictly anaerobic environment of predominantly carbon dioxide (CO_2) and become under the influence of pH change (8). The process of larval exsheathment is thus of great interest because it marks the transition from the free-living to the parasitic stages of these parasites (13, 14).

The rumen is a strictly anaerobic environment enriched with a complex community of bacteria, protozoa, fungi, archaea and bacteriophages (15, 16). The role of rumen fluid and its ability to regularly induce exsheathment of infective larvae has been well documented (9, 17). Early reports that certain compounds, either inherently produced by the host animal or present as a by-product of the plant fibre degradation process, act to stimulate parasite larvae to exsheath within the rumen (18-20). However, the composition of rumen fluid is dynamic and the active components within rumen fluid that can be harnessed in a practical manner to cause parasitic exsheathment are yet to be discovered (21-25). Therefore, the identification of novel bioactive compounds that could either trigger exsheathment exogenously on pasture or act endogenously to inhibit the process all together across several species of internal parasitic nematodes, are of great interest. The main challenge in such endeavors is the identification of compounds from plant extracts or biofluids (26). Metabolomics is an emerging research area to semi-quantitatively measure small molecular metabolites in biological samples using high-throughput approaches (23, 27). Lipidomics, involves the profiling of lipids within biological samples (28), that are essential for the synthesis of enzymes including steroid hormones, molecules involved in the transmission of membrane signals, and for the transport of vitamins (29).

In this study, the basic principles of dialysis and three different extraction methods were applied to investigate the metabolites with varying chemical properties (i.e. polarity), present in three different fractions of the rumen fluid metabolomes and lipidome of pasture-fed sheep. Here, we present the first study using semi- and non-targeted multimodal approaches to elucidate the rumen fluid-derived trigger factors and secretome (i.e. released molecules, peptides/proteins, carbohydrates and lipids) of *H. contortus* larvae associated with exsheathment.

MATERIALS AND METHODS

Animal, Diet and Rumen Contents Sampling

Whole rumen content samples were collected post-mortem and pooled from five sheep grazing *ad libitum* on a ryegrass and clover pasture diet. Approximately 5 L of rumen contents were collected from each animal and filtered through 4 layers of cheesecloth (335 μm mesh) to remove the plant material present in the digesta (Figure 1A). The pH of each sample was determined immediately after sampling using a pH meter (6.6). Filtered rumen fluid was immediately processed so as not to alter the fermentative capacity of the ruminal fluid. The sampling was conducted in December 2018 at AgResearch Grasslands Research Centre (Palmerston North, New Zealand) under the approval of the AgResearch Grasslands Animal Ethics Committee.

Dialysis and Fractionation of Whole Rumen Content

A method was developed to acquire dialyzed rumen fluid (DRF) fractions that enrich for different sized components of rumen fluid for subsequent exsheathment activity testing, as well as metabolomics and lipidomics analyses (Figure 1B). DRF fractions based on three molecular weight cut-offs (MWCO) were obtained using Spectra-Por® Float-A-Lyzer® G2 dialysis systems with MWCOs of 20 kDa (Z726931, Sigma-Aldrich), 8-10 kDa (Z726605, Sigma-Aldrich) and 100 Da (Z727253, Sigma-Aldrich). Briefly, the pooled and filtered RF contents were mixed and divided evenly into four Schott gas washing bottles fitted with Drechsel type head connections (GL 14, DURAN). The analytic conditions *in vitro* were identical to the animal's physiological conditions, with a temperature of 39°C in anaerobic conditions obtained by insufflating a stream of O_2-free CO_2 inside the container with constant mixing. To obtain each DRF fraction, five replicates of each individual MWCO apparatus were dialyzed against 10mL of autoclaved phosphate buffered saline (1× PBS, 137 mM NaCl, 2.7 mM KCl, 8 mM Na_2HPO_4, and 2 mM KH_2PO_4, pH 7.4) buffer overnight at 39°C in a water bath. Additional

containers were prepared in parallel containing only PBS and distilled water as control treatments. The principles of dialysis allowed small compounds to migrate from high concentration (rumen fluid contents) to low concentration (dialysis systems containing saline). DRF fractions and samples of digesta obtained from different phases of the process were either used immediately for larval exsheathment *in vitro* testing, or snap-frozen in liquid nitrogen and kept on dry ice until long term storage at -80ºC.

Production and Procurement of *H. contortus*

All experimental procedures used in generating the parasite material for this study were approved by AgResearch's Grasslands Animal Ethics Committee under the Animal Welfare Act 1999 in New Zealand (AEC application number 13928). Pure cultures of *H. contortus* third-stage larvae (L3) were maintained by regular passage through five otherwise parasite-free lambs housed indoors at the AgResearch's Grasslands campus. L3 were cultured in fresh faecal material containing eggs collected into faecal bags on infected sheep. Faeces were pooled and mixed with vermiculite then placed in trays, moistened with tap water (at 20℃), covered and cultured for 10 days at 22-24℃. A modified Baermann technique (30) was used to clean and separate the larvae from faeces. Briefly, approximately 150 g of faeces was enclosed in paper facial tissues and suspended over a large conical measuring flask filled with tap water. The samples were incubated for 20 hours and washed by their movement through the apparatus. The faeces were then removed and the liquid carefully siphoned to a remaining volume of about 20 mL. The resulting L3s and volume were examined in a counting chamber (Whitlock S.F.E.L.O., Australia; volume 2 mL) at ×100 magnification and stored in tap water at 10˚C until required. A single batch of larvae were used for all experiments to account for any batch-related confounding factors with larval viability and motility checked microscopically prior to any further experimentation. The specificity of genomic DNA was verified by automated sanger sequencing of the second internal transcribed spacer (ITS-2) of nuclear ribosomal DNA

following PCR amplification from genomic DNA (31). A 100% similarity identity was achieved corresponding to the *H. contortus* NZ_Hco_NP (genome version 1.0, BioProject accession number PRJNA517503), the representative chromosome-level genome of the anthelmintic-susceptible *H. contortus* field strain isolated from pasture-grazed New Zealand sheep (32-35).

In vitro Larval Exsheathment Assay

Prior to *in vitro* testing, pooled L3 cultures were cleaned and acclimated overnight to room temperature by gravity migration filtration into autoclaved PBS solution through nylon mesh (pore size 20 μm). Larval viability and motility were checked microscopically and quantified using a Petroff-Hausser chamber (Hausser Scientific) according to the manufacturer's instructions.

In this study, we report a 'closed' and high-throughput system originally designed to simulate the physiological conditions of the rumen (39°C and high CO_2 concentration) for the purposes of culturing rumen microorganisms (16, 36-40). This closed system has been modified to be used for *in vitro* larval exsheathment assays and is also suitable for future parasite-host-microbiome interactions and multi-omic studies (Figure 1D). As control treatments, dH_2O or anaerobic 1× PBS solution (137 mM NaCl, 2.7 mM KCl, 8 mM Na_2HPO_4, and 2 mM KH_2PO_4, pH 7.4) was mixed in boiling dH_2O and cooled to room temperature under a continuous flow of O_2-free CO_2. Once cooled, the PBS solution was transferred to 100 mL serum bottles in 70 mL aliquots and flushed with CO_2 for 1 h. The bottles were sealed with butyl rubber bungs and sealed with aluminium crimp caps before being autoclaved at 121ºC for 20 min. The DRF fractions were also transferred to serum bottles, flushed with CO_2 and sealed as described above, but not autoclaved prior to use.

Larval cultures were transferred anaerobically (approximately 200,000 L3/sample) using a O_2-free CO_2-flushed 3 mL syringe and wide bore hypodermic needle (16 G thickness and length

of 1-1/2 inch, BD), into aluminium-wrapped and pre-warmed serum bottles containing 70 mL of autoclaved PBS, and incubated anaerobically at 39ºC with gentle horizontal shaking at 75 rpm for 12 h in darkness. For each treatment, five biological replicates and three technical replicates were performed.

Exsheathment was determined by either complete or partial loss of the sheath and was measured by sub-sampling each replicate at 0 h (t=0) and after 12 h incubation at 39°C and CO_2 anaerobic conditions. At each time point, contents were thoroughly mixed before 1 mL was transferred using a O_2-free CO_2-flushed 1 mL syringe and wide bore hypodermic needle to a 24-well plate and exsheathment enumerated. Each subsample was quantified as previously described and larval density was diluted using PBS and 100 µL was transferred to another 24-well plate containing 900 µL dH_2O to yield approximately 200 larvae per replicate. Larvae were killed by the addition of 1 drop of 3% Helminthological iodine solution (Lugol's solution) and exsheathment enumerated.

Extractions for Metabolomics and Lipidomics Analyses

A combination of multiple complementary metabolomics platforms, or 'multi-modal' strategy, were applied in parallel to the same batch of biological samples to facilitate interpretation and provide extensive coverage of the exsheathment metabolome. To comprehensively elucidate the lipid and central carbon metabolism associated with exsheathment we applied: hydrophilic interaction liquid chromatography-mass spectrometry (HILIC-MS) to analyze polar compounds (41), ultra-high-performance liquid chromatography (UHPLC) and gas chromatography-mass spectrometry (GC-MS) systems to analyze lipids (LIPID), polar and semi-polar (C18) compounds analytical streams (42, 43), in both positive and negative mode electrospray ionization (ESI) modes.

Upon collection, the DRF fractions were snap-frozen in liquid nitrogen, transferred to glass vials and stored at -80°C until further use. Seven aliquots of 1 ml each (5 for analyses and two

for QC) of each sample were transferred into microcentrifuge tubes. The two QC samples (44) were pooled and solely used for monitoring sample degradation, tracking run-order effects within a batch, and quality control purposes only. Features of the samples can be found in Supporting Information Table S1. An overview of the extraction protocol and treatment of samples in preparation for metabolomics and lipidomics analyses is shown in Supplementary Figure S1. Briefly, samples were thawed overnight at 4°C, centrifuged (4°C, 11,000 × *g*) for 10 min and 200 µl of supernatant transferred into a 2 mL micro-centrifuge tube. An extraction solvent comprising 800 µl of chloroform:methanol (1:1; v/v) was added and samples were vortexed (1 min). Sample was diluted with water (400 µl), again vortexed (1 min), and centrifuged (4°C, 11,000 × *g*) for 15 min.

To evaluate the lipidome of the DRF fractions, the lower, organic layer was taken (200 µl) separately, evaporated to dryness under a continuous stream of nitrogen (30°C), and the dried extract was reconstituted in 200 µl of chloroform:methanol (2:1; *v/v*), with 16:0 d_{31}-18:1 phosphatidylethanolamine (10 µg/mL) as an internal standard. Finally, samples were vortexed (1 min), and 100 µl was transferred to a glass insert in an auto-sampler vial for LC-MS analysis. For polar and semi-polar compounds, hydrophilic interaction liquid chromatography (HILIC) and C18 chromatography were applied, respectively (41-43). For these analyses, all procedures were similar to that of lipids, except that the extraction solvents comprised of acetonitrile:water containing 0.1% formic acid (1:1 for HILIC and 1:9 for C18, *v/v*).

Chromatography and Mass Spectrometry Conditions

The chromatographic gradient and other conditions for lipid analysis have been previously described (42, 45). For semi-polar compounds, C18 conditions were set as described (42, 43) by extract (2 µL) was injected into a 100 mm × 2.1 mm Thermo Hypersil Gold C18 column with 1.9 µm particle size and eluted over a 16 min gradient with a flow rate of 400 µL/min. The mobile phase was a mixture of water with 0.1% formic acid (solvent A), and acetonitrile

with 0.1% formic acid (solvent B). Chromatographic gradient and other LC-MS conditions have been previously described (43, 46). For polar compounds, HILIC conditions were set as described (41) by extract (2 µL) was injected into a 100 mm × 2.1 mm ZIC-pHILIC column with 5 µm particle size and eluted over 17 min with solvent gradient from 97% solvent A (1 min), 97%-70% solvent A (1-12 min), 70-10% solvent A (12-14.5 min) to 10% solvent A (14.5-17 min). Mobile phase solvent A was a mixture of acetonitrile with 0.1% formic acid, solvent B was a mixture of water with 16 mM ammonium formate and flowrate was 250 µL/min. Chromatographic gradient and other LC-MS conditions have been previously described (41, 45).

C18 and HILIC column effluents were connected to a high-resolution, accurate mass Exactive mass spectrometer with Orbitrap™ technology, and lipid analysis was conducted on a Q-Exactive mass spectrometer. All samples were analysed in negative and positive ionisation modes. Pooled sample from all conditioned DRF fraction extracts and internal standards were used to maintain the data quality in both positive and negative mode analyses. Moreover, samples were randomised prior to injection to avoid any systematic effects.

Data Processing and Analysis

The metabolomics workflow comprises of a series of steps starting from raw data, leading to data processing, statistical analysis, visualization and compound identification (Supplementary Figure S2). The time-consuming and labor-intensive processes of metabolite feature extraction, alignment, identification and statistical analysis, were streamlined by utilizing the publicly available XCMS Online (47) and MetaboAnalyst (48) bioinformatics tools. The MS raw data files (Thermo .raw files) were converted to mzXML files using MSConvert function of ProteoWizard™. These files were uploaded to XCMS Online (49) for data processing including peak detection, retention time alignment, profile alignment, isotope annotation, grouping and gap filling.

Relative quantification of metabolite features was based on extracted ion chromatogram (EIC) areas, with the Kruskal Wallis statistical test used to find the metabolic differences. All classes other than the deuterated species were selected. The type of adducts generated are dependent on the solvents and eluting conditions used. For this study, $[M-H]^-$ and $[M+Cl]^-$ adducts, and $[M+H]^+$, $[M+Na]^+$, $[M+NH_4]^+$, $[M+H-H_2O]^+$ and $[M+]^+$ adducts were selected for negative and positive ionisation modes, respectively. Finally, a retention time tolerance of 0.01 mins, and mass error tolerance of ± 10 ppm was allowed. Results/identifications were concatenated into a single table and matched with the respective, normalised, peak intensity table (Supplementary Table S1-3). A multi-group comparison between the three DRF fractions (20 kDa, 8-10 kDa and 100 Da) and PBS control versus the blank samples was performed, focusing only on features identified with *m/z* attributes that were significant (FDR p value < 0.05) between the groups. The filtered matrix was normalized by a QC based robust LOESS signal correction (QC-RLSC) (50) and all subsequent *m/z* features with relative standard deviation (RSD) (51) > 0.3 were eliminated. The resultant data matrix was used for downstream statistical analyses and metabolite identification.

Following the metabolomics data analysis pipeline (52) the raw data from the LIPID stream (Figure 1E) were processed and subjected to peak detection, quality control, statistical analysis of detected peaks, and the annotation of top-ranking peaks. On the annotation side, because only sparse fragmentation spectra (MS2) were collected for positive mode ions and no MS2 for negative mode ions in this study we leverage the correlation structure of peaks for metabolite identification (52). Unless otherwise specified, we carry out MSI (Metabolomics Standards Initiative) level 2 metabolite annotation as evidenced by chromatographic behavior, library search based on accurate mass (< 10 ppm error) and the match of isotopic peak intensity between experimental and theoretical spectrum.

Regarding the C18 and HILIC streams (CP and HP represent positive ionisation mode, CN and HN represent negative ionisation mode), after the filtering of ^{13}C isotopic peaks and early eluting peaks (<1 min) in C18, 72 CP peaks and 72 CN peaks were left for peak annotation. Metabolite identification was based on the match of m/z ($[M+H]^+$ or $[M-H]^-$, within 5 ppm accuracy) with those in HMDB, and the retention time with in-house databases for C18 and HILIC chromatographic conditions. Moreover and unlike the LIPID stream, MS2 data were not explored for these datasets as plausible annotations were reached strictly based on accurate mass and retention time. We exploited the correlation structure of top peaks to assist the annotation. Correlated peaks due to coelution may indicate the similar physio-chemical properties of eluting metabolites, or in-source fragment ions. The presence of in-source fragment peaks helps identify the molecular ion for correct annotation of the metabolite (52). On the other hand, peak correlation among biological samples may suggest the origin of candidate metabolites, providing additional information for annotation (Supplementary Figure S3).

Statistical Analysis and Metabolite Annotation/Identification

Metabolite features were confirmed by matching experimental tandem MS^1 and source-induced fragmentation data against standard MS/MS spectra in the METLIN MS^2 spectral library using XCMS Online (47, 53). Prior to multimodal analysis and pathway prediction, the appropriate fold change (FC $\geq$ 2), *p*-value ($p < 0.1$), and intensity thresholds (10,000) for multimodal analysis were defined. Significantly differential metabolites were further determined from the exact mass composition using HMDB (54), LIPID MAPS (55), METLIN (53), PubChem and mzCloud databases. The MS data and metadata reported in this study have been submitted to the MetaboLights database (www.ebi.ac.uk/metabolights) with the study identifier: MTBLS1717.

Both univariate and multivariate data analyses were also conducted. Unsupervised multivariate analyses of the metabolites was done using principal component analysis (PCA) to highlight any potential clustering of the groups based on maximizing the variation inherent in the data. Supervised clustering was carried out using partial least square-discriminant analysis (PLS-DA). Briefly, each data set was summarized into much fewer variables or scores that were weighted averages of the original variables and analyzed in reduced multivariate space against different weighting profiles or loadings to identify variables that contribute the most to a particular score and/or treatment group. Univariate hypothesis testing of the data was carried out using Permutation ANOVAs as implemented in the lmPerm R package version 2.1 (56) with 1 million permutations, after which, significance was determined for the metabolites using the Benjamini-Hochberg FDR-corrected (57) p-values. Significance of metabolites between treatments were determined using FDR-corrected permutation tests perfomed using the "independence_test" function in the coin R package version 1.3-1 (58). Finally, the metabolomic data sets were integrated automatically, followed by the prediction of dysregulated metabolic pathways using Mummichog (59) and MetaboAnalyst 4.0 (48). In addition, statistical analyses were performed using in-house scripts in R (60) with appropriate parameters and an online chemometric analysis suite, MetaboAnalyst 4.0 (48).

Results

DRF Fraction Activity on Third-Stage Larval (L3) Exsheathment in *H. contortus*

The *in vitro* exsheathment assays showed that the efficacy of DRF on larval exsheathment increased as the DRF fraction sizes decreased (Figure 1D). The efficacy of DRF was determined by measuring the percentage of larvae that exsheath at 39°C and an anaerobic environment (CO_2), and then in the absence of rumen conditions on freshly cultivated *H.*

contortus L3s. Overall results post 12 hr incubation were as follows: distilled water negative control (0%), saline positive control (68%), raw rumen fluid (85%), 20 kDa DRF (62%), 8-10 kDa DRF (80%) and 100 Da DRF (97%). In the absence of rumen conditions, there was no exsheathment observed across any of the DRF fractions. The relatively low amount of exsheathment observed using the 20 kDa DRF leads us to propose that this fraction may contain large compounds with inhibitory effects on larval exsheathment, not present in the smaller DRF fractions.

Multivariate Analysis of DRF Fractions Identified Distinct Metabolite Groups

For identifying exsheathment biomarker candidates, metabolites with an FDR corrected *p* value of less than 0.05 and fold change of at least one was deemed to be significantly different between the PBS control and DRF (20 kDa, 8-10 kDa, 100 Da) groups and selected for further analysis. The normalized peak tables of metabolites passing these criteria are described in Supplementary Tables S1-S3. Peak names were denoted with 'P' and 'N' from positive (HP, CP, LP) and negative (HN, CN, LN) ionization mode peaks, respectively. After data processing, filtering and normalization, a large number of unknown peaks that may correspond to unique metabolic features include 981 C18 (644 CP and 337 CN), 314 HILIC (156 HP and 158 HN) and 1,421 LIPID (1,259 LP and 162 LN) were identified via XCMS and LipidSearch, and not further described in this work but warrant future investigation. In contrast, the multi-modal analysis of our MS data detected a total of 447 C18 (270 CP and 177 CN) and 176 HILIC (76 HP and 100 HN) top metabolite features or peaks with putative METLIN annotations that have been used for all subsequent analyses (Tables S1-3). The PLS-DA modeling and scores plots revealed clear separation between the PBS control and DRF fraction treatment groups based on their expression (Figure 2). Furthermore, the PLS-DA analysis revealed that the clear clustering between DRFs (20 kDa, 8-10 kDa, 100 Da) and PBS control

groups was consistent for every metabolomics stream applied. Overall, the PLS-DA findings provide validation that ruminal biochemistry changed according to DRF classification and that our experimental design has managed to capture the treatment effect pattern.

Our analyses of the LIPID data revealed a total of 44,218 LP and 21,056 LN peaks were obtained. The missing values of peak intensity were replaced by the half of the lowest peak intensity among samples. Only peaks eluting between 1 ~ 13 min were retained. The merge of ^{13}C isotopic peaks and the correction of run order effects were implemented here (as in Cao et al. 2017). After the filtering process, 28,664 LP peaks and 13,629 LN peaks were left for statistical investigation. PCA analysis showed that the 20 kDa fraction (DRF1) was distinct in lipid profile from other fractions, where no difference among themselves. With supervised PLS-DA PBS is also separable from other fractions using LP peaks (Supplementary Figure S4A). Empirical Bayes moderated F-test was implemented using the R limma package (61), and then deployed to select to LP and LN peaks relevant to the DRF1-3 fraction groups and PBS (Supplementary Figure S4B-C). With the criterion of FDR adjusted *p*-values < 0.01, 421 LP peaks and 33 LN peaks were selected for peak annotation. Hierarchical clustering of these top peaks based on Pearson's correlation coefficients was performed as co-eluting metabolites or in-source fragment peaks are often correlated among samples. We exploited such information to facilitate annotations.

Overall, the fragmentation data provided rich information for the annotation of metabolite species (Table 1).

A prerequisite for our comparative multimodal analyses was that a metabolite needed to be present in ≥ 3 biological replicates post exsheathment across all metabolomics streams. A total of 1,087 metabolites with putative annotations representing the exsheathment developmental stage (i.e. L3 to xL3) of *H. contortus* were quantified with varying degree of confidence and

selected as the basis for all subsequent analyses. In contrast, a total of 1,454 metabolites with no current putative or unknown annotations were identified across all metabolomics streams. Additional multivariate analyses were employed to simultaneously identify the metabolites whose expression can separate the PBS control from the DRF fraction groups and best explain any variance within the various metabolomics streams datasets. Most (n = 1,028; 94.6%) metabolites were present in ≤ 2 distinct metabolomics streams, whereas 36.1% (n = 392) of metabolites were detected in >2 streams (Figure 3). The numbers of unique quantified metabolites from negatively ionized streams in *H. contortus* xL3s were highest in the LIPID ($LIPID^-$; n =231), followed by $C18^{+/-}$ ($C18^-$; n = 43) and HILIC ($HILIC^-$; n =20), with 28 core metabolites identified (Figure 3A). In comparison, the LIPID ($LIPID^+$; n =335) were still highest, followed by C18 ($C18^+$; n = 60) and HILIC ($HILIC^+$; n =6) unique metabolites from positively ionized streams, with 31 core metabolites identified (Figure 3B). For both positively and negatively ionized streams the greatest number of unique metabolites were identified for $LIPID^{+/-}$ (n = 213), whereas only one and twelve unique features were present in the $HILIC^{+/-}$ and $C18^{+/-}$ streams, respectively (Figure 3C). Overall, only six metabolites were detected in all metabolomics streams (Figure 3C), these include: 2-carboxy-4-dodecanolide, 3',4'-methylenedioxy epicatechin 5,7-dimethyl ether, 7-acetyloxy-2-methylisoflavone, dodecanedioic acid, koparin 2,3-dimethyl ether and zebularine, but warrant further investigation and characterization.

Encouraged by our PLS-DA and multivariate analyses, we performed hierarchical clustering to test if the DRF groups can be separated by unsupervised statistical techniques (Supplementary Figure S5). Clustering the DRF groups by the top 50 metabolites resulted in strong groupings of each DRF fraction across each stream, which was to be expected with the majority of the metabolites being specific between the ionization groups. Overall, >85% of the top 50 putative metabolites were upregulated in the 20 kDa fraction for each stream. Common

expression patterns for putative metabolites were identified for the smallest pore size MWCO of 100-150 Da and the PBS control groups across all metabolomics streams. The DRF fractions from the larger MWCOs, 8-10 and 20kDa, also displayed common expression patterns mainly for HILIC$^{+/-}$ (Supplementary Figure S5A and B) and half of metabolites in C18$^{+/-}$ (Supplementary Figure S5C and D), but to a lesser extent in the 8-10kDa groups.

The resulting subset of samples was selected to illustrate the application of our multi-modal approach to annotate statistically significant peaks differentiating between the various DRF and PBS treatment groups. Clustering analysis of top peaks revealed one group of peaks high in DRF1 and another higher in PBS (Figure 4 and Table 1). High in DRF1 are the secondary metabolites of plant origin with amino acids high in the PBS control group. Metabolite identification was based on accurate m/z, retention time and sometimes its presence in multiple platforms (Table 1). Of interest and among the top HN peaks, Lactic acid ($C_3H_6O_3$) or HN89.0235_2.73 was annotated as lactic acid $[M-H]^-$, within 4.2 ppm error from the computed mass. The retention time was largely matched to the standard (2.14 min) from our in-house HILIC database. The distribution of lactic acid among the four treatment groups is shown in Figure 4B. However, a large proportion of peaks remained unknown and warrant future detailed investigations from raw data. For example, a group of statistically significant HN peaks eluting after 12 min and that did not correspond to a plausible hit from HMDB and PlantCyc database by mass alone were identified (Supplementary Figure S6).

Overall, the LIPID top peaks formed three distinct peak groups (Figure 4C and D), where 62 peaks from the group 1 are abundant in the PBS fraction; 23 peaks from group 2, and the largest peak group are high in DRF1 (20 kDa). Based on the annotation triglycerides (TGs) were abundant in PBS; some phosphatidylcholines (PC 32:5, PC 34:5, PC 35:5) were increased in DRF2 and DRF3. Molecular species in the largest group 3 shared the same pattern, where they were abundant in DRF1 but low or non-detected in other fractions. The group 3 metabolites

annotated in this group include LPG, DG and plant sterols. We have also investigated MS2 spectra collected for a few precursor *m/z* using the previously described method (62). For example, the peak LP614.572_8.62 ($[M+NH_4]^+$) was further annotated as DG 16:0_18:0 with the chain structures characterized (Supplementary Figure S7), along with the information of accurate mass and retention time. On the contrary to DG37:1 (LP654.6034_8.61), this saturated glycerolipid was the lowest in DRF1.

Identification of Exsheathment Associated Metabolites

To tease out the natural metabolites that constitute the exsheathment fluid secreted by the larvae upon ecdysis, metabolite expression and clustering between the different ionization groups and metabolomics streams were investigated and characterized (Table 1 and Figure 4). Furthermore, in order to expand on the inferred KEGG metabolic pathway annotations, the module of enrichment analysis of MetaboAnalyst based on the SMPDB (The Small Molecule Pathway Database) was investigated. Among these were a panel of metabolites including methionine, leucine, alanine, phenylalanine, xanthine and hypoxanthine, that were significant in two separate metabolomics streams and associated with amino acids as well as purine and pyruvate metabolism pathways. Furthermore, of the five lipid classes identified by the non-targeted lipidomics stream, concentrations of the triglycerides C16:0 C18:0, C48:1, C54:4 and C52:1 were high in the PBS control group.

Discussion

Early work exploring the effects of the fundamental anaerobic (CO_2) and temperature (40 °C) rumen conditions on exsheathment of a variety of nematode species (9-11), formed the conceptual basis for this work. The initial biological objective of this study was to validate and determine the efficacy of DRF fractions on larval exsheathment using our *in vitro* exsheathment system that mimics inoculation of *H. contortus* L3 larvae into the rumen. To date, in order to

obtain xL3s for numerous gastrointestinal nematodes (GIN) parasite species it is common laboratory practice to use sodium hypochlorite as a desheathment agent (14, 63-65). The developed 'closed' *in vitro* exsheathment system presented in this work provides an effective alternative method for larval exsheathment. Our straightforward system maintains a constant and measurable anaerobic environment that does not damage the larvae, enables subsampling without altering the *in vitro* conditions, and can be tailored to accommodate future omics'-oriented studies (66). Indeed, our results showed that larval exsheathment increased as the DRF fraction sizes reduced which called for further investigation and interpretation at the molecular level. However, until now, metabolomic studies focusing on GIN biology and *H. contorus* life cycle development remain largely uncharted territory.

While rapid developments of the 'omics field have accelerated our knowledge of nematode biology at the molecular level, much fewer advancements have been made for parasitic nematodes of veterinary importance and particularly regarding metabolomics. In this study, numerous analytical techniques and methodologies have been explored to carry out metabolomic profiling to investigate the effects of various DRF fractions on larval exsheathment in *H. contortus*. The discovery of novel or identification of pathophysiological biomarkers that cause infective L3s to exsheath/moult and develop to become infective, provide much needed opportunities for the development of novel drug or vaccine targets for the mitigation of haemonchosis. To investigate the biological mechanisms at play and identify potential nematode exsheathment bioactives, we applied the basic principles of dialysis combined with semi- and non-targeted multimodal metabolomics approaches. Based on the PLS-DA (Figure 2) and stringent statistical analysis (Figure 3) we first identified potential key metabolites related to *H. contorus* larval exsheathment in the rumen (Tables S1-3). The significant unique and mutual metabolites were then identified across all metabolomics streams

and DRF fractions (Table 1) to uncovered the molecular-level metabolic changes related to larval exsheathment.

Regarding general energy metabolism, robust changes of metabolite levels in larval exsheathment included increased L-lactic acid (Figure 4B and Table 1), a significant substrate of pyruvate metabolism and in particular gluconeogenesis. Early and only available studies examining the specific end product patterns of *H. contortus* concluded that only traces of lactate are excreted, with the main end products being acetate, propionate and propanol (67-69). However, these studies were all based on adult nematodes with the production and/or ability to utilize lactate being a major potential advantage and mechanism of pathogenicity within the host for this GIN parasite. Although direct lactate production as a anaerobic fermentation end product was not assessed as part of this study, genes associated with an alternative glycolytic pathway, the methylglyoxal shunt, for the alternative production of lactate are all present within the *H. contortus* NZ_Hco_NP (v1.0) genome (32). These genes encode for the enzymes: fructose-1,6-bisphophate aldolase (*fbp*), methylglyoxal synthase (*mgsA*), glyoxylase (*gloA/B*), S-lactoylglutathione hydrolase, and D-lactate dehydrogenase (*ldhD*), converting D-fructose-1,6-bisphophate to pyruvate. Moreover, the genes encoding both forms of lactate dehydrogenase (*ldhD* and *ldhL*) in which the *ldh* gene encoding L-lactate dehydrogenase plays a key role in the production of L-lactate from pyruvate, have been identified. Interestingly, the lactate racemase gene that is responsible for the conversion of D-lactate to L-lactate, appears to be missing from the *H. contortus* NZ_Hco_NP (v1.0) genome. For future work, the developed *in vitro* system should be used to determine the relative abundances of the lactate isoforms produced during larval exsheathment under basic rumen conditions.

In addition to the production of lactate, the metabolites alanine, xanthine, hypoxanthine, succinate, flavonoids (hydroxy dimethoxy flavone) and various triglycerides were also significantly upregulated in *H. contortus* xL3. This particular group of metabolites is associated

with the ‘Warburg effect’ (SMP0000654) that is a metabolic response to an increase of the glycolytic flux due to hypoxia or a strictly anaerobic environment (70). The Warburg effect is also referred to as aerobic glycolysis and is a rather inefficient means of ATP production (~4 mol ATP/mol glucose) when compared to the tricarboxylic acid (TCA) cycle (~36 mol ATP/mol glucose) which is the primary aerobic metabolism of larvae. However, anaerobic glycolysis accounts for at most ~2 mol ATP/mol glucose and may account for the metabolic advantage that the Warburg effect confers to GIN larvae upon transition into the rumen. While it is tempting to postulate that this alternative pathway supports the proliferation of cells throughout the various larval stages while out on pasture by facilitating the uptake and utilization of available nutrients by generating energy for regulating various signaling and metabolic pathways. Further transcriptomic evidence is required to investigate such hypotheses in GIN nematodes and shed light on the possible role of this alternative metabolic pathway, particularly with regards to dauer and over-winter survival strategies.

Moreover, the above-mentioned metabolites were identified among the most abundant metabolites across all streams and are directly related to glycolysis *via* numerous carbohydrate sources. Examples of such simple carbohydrate sources that are made available in the rumen via microbial degradation of the plant material include; fructose, galactose, mannose and sucrose, with also complex sugar substrates such as starch and inositol. Such carbohydrate sources are readily available to the larvae within the rumen as bi-products of microbial plant fibre degradation (16, 39, 40, 71). While the current metabolomics approach was not appropriate for the detection of carbohydrates, optimization of the reported metabolomics pipelines will be a focus for future investigations. Characterization of the larval initial uptake compensated by the activity of various transporters and subsequent utilization of both simple and complex carbohydrate sources, requires further transcriptomic investigation that is a focus of our upcoming research.

In addition to the confronting physiochemical environmental conditions associated with migration into the rumen such as such as temperature, pO_2, pCO_2, pH, osmotic pressure and redox potential (72), parasitic nematodes are able to extract most of their nutritional requirements from the environment to meet the energy requirements of exsheathment (73). Changes of amino acids in larval exsheathment (PBS control group) were also observed and include methionine, leucine, alanine and phenylalanine (Table 1). The complex and essential amino acid methionine which animals cannot synthesize and the branched-chain amino acid (BCAA) leucine were identified in both the C18 and HILIC streams with high confidence. These amino acids were included in significantly changed KEGG pathways such as aminoacyl-tRNA biosynthesis (cel00970), biosynthesis and degradation of BCAAs (cel00290), as well as the cysteine and methionine metabolism (cel00270) in nematodes. Recent metabolomics studies have consistently revealed that BCAAs are positively related to longevity common to dauers in worms (74, 75) and proposed to be intricately associated with mitochondrial biogenesis during exsheathment. Alanine was also identified as upregulated in the alanine, aspartate and glutamate metabolism KEGG pathway (cel00260), that is involved in the protein synthesis and synthesis of other vital amino acids (glycine, serine, threonine, etc.), phospholipid and collagen production, as well as in release of energy, all of which have important roles in rapid cell proliferation. Therefore, the increased levels of particular BCAA profiles, may serve as potential biomarkers of parasitism in the rumen and possibly other tissue types. Furthermore, our study further validates methionine as a rational candidate for development of anti-parasite drugs and topically applied pasture nematicide (76).

In this report we applied the first known lipidomic approach to describe the rumen fluid-derived trigger factors and secretome of *H. contortus* L3 larvae associated with exsheathment, an essential transition from aerobic free-living to anaerobic parasitic stages. A total of 16 lipid species across five classes have been identified with high confidence that formed three types

of metabolite groupings. In accordance with a recent report on the global lipidome of *H. contortus* (77), long chain (more than 12 carbons) saturated fatty acid levels are high in the transition from the free-living phase. The group 2 lipid species were represented by glycerophosphocholine lipids (PCs) associated with the glycerophospholipid metabolism (cel00564) KEGG pathway and the SMPDB pathways including phospholipid biosynthesis (SMP0000025) as well as retinol or vitamin A metabolism (SMP0000074). All of which are related to choline metabolism covering phosphorylcholine, dihydroxyacetone phosphate, and glycerophosphocholine that is a choline derivative and one of the major forms of choline storage. Choline degradation leads to generation of sarcosine (*N*-methylglycine), a natural amino acid found in numerous mammalian tissues that acts as an intermediate metabolite and is intricately linked to glycine degradation (78, 79). Sarcosine can also be generated by alternative pathways *via* creatine metabolism (80). Interestingly, cyclocreatine is a creatine analog and was detected in all DRF fractions using the $C18^{+/-}$ and $HILIC^{+}$ streams (Supplementary Tables S1 and S2). Cyclocreatine can regulate creatine biosynthesis by suppressing the level of arginine and glycine amidinotransferases, and is able to cross various membranes including the blood brain barrier. Recently, it has been reported that both *H. contortus* and *T. circumcincta* preferentially utilize phosphoarginine oppose to phosphocreatine as an energy buffer for nitrogen metabolism (81, 82). Furthermore, creatine is phosphorylated and dephosphoryated by mitochondrial and cytosolic creatine kinase and creatinase that also serves to protect against inhibition of mitochondrial respiration. Multiple copies of both creatine metabolism enzymes are present in the *H. contortus* NZ_Hco_NP (v1.0) and may convey an obvious advantage to the ingested L3 as they are able to utilise the host creatine as a source of nitrogen *via* sarcosine generation from creatine and the breakdown of sarcosine by sarcosine oxidase to glycine. As such nematode phosphagens and kinases may

serve well for future development as anthelmintic targets and as potential vaccine candidates due to their strong antigenicity in mammals.

With regards to group 1 lipid species associated with the control group containing only *H. contortus* xL3s in PBS and directly correlated to larval exsheathment, four major triglycerides (TGs) were identified. These include the branched fatty acid C48:1, linoleoyl dilein (C54:4), palmitoyl stearoyl olein (C52:1) and the more commonly known palmitic acid (C16:0) and oleic acid (C18:0). Our findings are in agreement with previous studies, particularly *C. elegans* (83, 84), that report the adaptation of nematodes to increase levels of saturated fatty acids at higher temperatures and in response to a change in their environmental temperature. A key unanswered question is whether our findings apply to other pathogenic nematodes of ruminants, with future efforts combining genomic and transcriptomic approaches needed to advance this issue.

While many of the biological functions of the group 1 metabolite species associated with the PBS only control samples identified with our multi-modal metabolomics analysis remain uncharacterized, there are some exceptions that warrant further investigation. For example, juvenile hormones (JH) (85, 86), more specifically 10S-juvenile hormone III diol, was identified as a significant metabolite in both the $C18^{+/-}$ and $HILIC^{-}$ streams and corresponds to the insect hormone biosynthesis (cel00981) KEGG pathway. JH have been well characterized as an important part of the normal ecdysis cascade through the stimulation of the neuroendocrine system of the worm, resulting in the production and release of the molting or exsheathment fluid (87, 88). The presence or absence of JH has downstream effects on numerous biochemical pathways such as metamorphosis, reproduction and diapause. The robust detection of such a metabolite using our *in vitro* system warrants further work to investigate the associated gene expression profiles.

Conclusion

In this study, we validated our 'closed' *in vitro* exsheathment system that provides an effective alternative method for larval exsheathment suitable for many different future omics'-oriented applications. Our study not only established robust multivariate analysis models that could discriminate among various DRF fractions metabolomic profiles, but also identified robust metabolic signatures that may be used as potential biomarkers of larval exsheathment based on different statistical models. In conclusion, this is the first study to report the use of a comprehensive multimodal metabolomics approach with great potential for the discovery of new biomarkers for nematode parasitism and provides a valuable resource for future mining of novel anthelmintic targets and potential vaccine candidates. The small sample size our research could serve as a platform study for future functional metabolomics studies investigating larval exsheathment and development. When coupled with the advent of sequencing technologies and availability of genomic and transcriptomic datasets, is a comprehensive approach for the identification of these metabolites and characterization of the exsheathment molecular mechanisms. Integration of the metabolic data with the recent chromosome-level genome sequence of the anthelmintic-susceptible New Zealand *H. contortus* NZ_Hco_NP field strain, will aid to broaden the analysis repertoire. Overall, the metabolites identified under basic rumen conditions coupled with the *H. contortus* NZ_Hco_NP field strain genome enables future research to explore the nexus of gene-environment interactions associated with exsheathment to guide the development of precision intervention strategies (i.e. novel drug and vaccine targets) against major parasitic nematodes. Research in this space is important owing to the diminished efficacy demonstrated for both old and new anthelmintics in parasitic nematodes and their effect on livestock in NZ and around the world.

Data Availability Statement

The datasets presented in this study can be found in online repositories. The names of the repository/repositories and accession number(s) can be found in the article/supplementary material.

Ethics Statement

The animal study was reviewed and approved by the AgResearch Grasslands Animal Ethics Committee, Palmerston North, New Zealand. Written informed consent was obtained from the owners for the participation of their animals in this study.

Author Contributions

NP conceived the project, designed and conducted all experiments, analyzed and interpreted the data, and wrote the manuscript. PHM provided statistical and bioinformatics support for the project. AKS and MC provided guidance with metabolomics and lipidomics analysis. All authors critically revised and approved the final manuscript.

Conflict of Interest Statement

The authors declare that the research was conducted in the absence of any commercial or financial relationships that could be construed as a potential conflict of interest. Author NP was employed by the company AgResearch Ltd. The remaining authors declare that the research was conducted in the absence of any commercial or financial relationships that could be construed as a potential conflict of interest.

Acknowledgments

Special thanks to Linley Schofield in the Rumen Microbiology lab for providing the dialysis equipment. We thank Hailey Gillespie and Trevor Holloway for their timely assistance with

the collection of rumen fluid for this study. We thank Richard Scott and Dave Leathwick for their helpful feedback in the early stages of this project, also Alastair Ross and Karl Fraser for their revisions on the manuscript. This study was supported by the AgResearch Ltd Strategic Science Investment Fund (SSIF), contract C10X1702 to NP. This work was also supported in part by the Agricultural and Marketing Research and Development Trust (AGMARDT) Postdoctoral Fellowship Programme, Grant P17001 to NP.

Supplementary Material

The Supplementary Material for this article can be found online at: ######################.

References

1. P. M. Jourdan, P. H. Lamberton, A. Fenwick and D. G. Addiss: Soil-transmitted helminth infections. *The Lancet*, 391(10117), 252-265 (2018)
2. J. Charlier, M. van der Voort, F. Kenyon, P. Skuce and J. Vercruysse: Chasing helminths and their economic impact on farmed ruminants. *Trends in parasitology*, 30(7), 361-367 (2014)
3. T. Evans and N. Chapple: The animal health market. *Nature Reviews Drug Discovery*, 1(12), 937-938 (2002) doi:10.1038/nrd975
4. R. Besier, L. Kahn, N. Sargison and J. Van Wyk: Diagnosis, treatment and management of *Haemonchus contortus* in small ruminants. In: *Advances in Parasitology*. Elsevier, (2016)
5. R. M. Kaplan and A. N. Vidyashankar: An inconvenient truth: global worming and anthelmintic resistance. *Veterinary parasitology*, 186(1-2), 70-78 (2012)
6. T. G. Geary, J. A. Sakanari and C. R. Caffrey: Anthelmintic drug discovery: into the future. *J Parasitol*, 101(2), 125-33 (2015)
7. A. Kotze and R. Prichard: Anthelmintic resistance in Haemonchus contortus: history, mechanisms and diagnosis. In: *Advances in parasitology*. Elsevier, (2016)
8. D. L. Lee: Cuticle, moulting and exsheathment. *The biology of nematodes*, 171-209 (2002)
9. W. Rogers: The physiology of infective processes of nematode parasites; the stimulus from the animal host. *Proceedings of the Royal Society of London. Series B. Biological Sciences*, 152(948), 367-386 (1960)
10. R. Sommerville: The exsheathing mechanism of nematode infective larvae. *Experimental parasitology*, 6(1), 18-30 (1957)
11. A. Taylor and J. Whitlock: The exsheathing stimulus for infective larvae of *Haemonchus contortus*. *Cornell Veterinarian*, 50(3), 339-344 (1960)
12. A. P. Page and I. Johnstone: The cuticle. *WormBook* (2007)
13. W. Rogers and R. Sommerville: The physiology of the second ecdysis of parasitic nematodes. *Parasitology*, 50(3-4), 329-348 (1960)

14. P. H. Silverman and K. R. Podger: *In vitro* exsheathment of some nematode infective larvae. *Experimental Parasitology*, 15(4), 314-324 (1964)
15. G. Henderson, F. Cox, S. Ganesh, A. Jonker, W. Young, G. R. C. Collaborators and P. H. Janssen: Rumen microbial community composition varies with diet and host, but a core microbiome is found across a wide geographical range. *Scientific reports*, 5(14567), 1-13 (2015) doi:10.1038/srep14567
16. R. Seshadri, S. C. Leahy, G. T. Attwood, K. H. Teh, S. C. Lambie, A. L. Cookson, E. A. Eloe-Fadrosh, G. A. Pavlopoulos, M. Hadjithomas, N. J. Varghese, D. Paez-Espino, N. Palevich, P. H. Janssen, R. S. Ronimus, S. Noel, P. Soni, K. Reilly, T. Atherly, C. Ziemer, A.-D. Wright, S. Ishaq, M. Cotta, S. Thompson, K. Crosley, N. McKain, R. J. Wallace, H. J. Flint, J. C. Martin, R. J. Forster, R. J. Gruninger, T. McAllister, R. Gilbert, D. Ouwerkerk, A. Klieve, R. A. Jassim, S. Denman, C. McSweeney, C. Rosewarne, S. Koike, Y. Kobayashi, M. Mitsumori, T. Shinkai, S. Cravero, M. C. Cucchi, R. Perry, G. Henderson, C. J. Creevey, N. Terrapon, P. Lapebie, E. Drula, V. Lombard, E. Rubin, N. C. Kyrpides, B. Henrissat, T. Woyke, N. N. Ivanova and W. J. Kelly: Cultivation and sequencing of rumen microbiome members from the Hungate1000 Collection. *Nature Biotechnology*, 36(4), 359-367 (2018) doi:10.1038/nbt.4110
17. A. DeRosa, S. Chirgwin, J. Fletcher, J. Williams and T. Klei: Exsheathment of *Ostertagia ostertagi* infective larvae following exposure to bovine rumen contents derived from low and high roughage diets. *Veterinary parasitology*, 129(1-2), 77-81 (2005)
18. T. Petronijevic and W. Rogers: Undissociated bases as the stimulus for the development of early parasitic stages of nematodes. *International journal for parasitology*, 17(4), 911-915 (1987)
19. T. Petronijevic, W. Rogers and R. Sommerville: Carbonic acid as the host signal for the development of parasitic stages of nematodes. *International journal for parasitology*, 15(6), 661-667 (1985)
20. T. Petronijevic, W. Rogers and R. Sommerville: Organic and inorganic acids as the stimulus for exsheathment of infective juveniles of nematodes. *International journal for parasitology*, 16(2), 163-168 (1986)

21. M.-Y. Xue, H.-Z. Sun, X.-H. Wu, J.-X. Liu and L. L. Guan: Multi-omics reveals that the rumen microbiome and its metabolome together with the host metabolome contribute to individualized dairy cow performance. *Microbiome*, 8, 1-19 (2020)
22. V. M. Artegoitia, A. P. Foote, R. M. Lewis and H. C. Freetly: Rumen fluid metabolomics analysis associated with feed efficiency on crossbred steers. *Scientific reports*, 7(1), 1-14 (2017)
23. F. Saleem, S. Bouatra, A. C. Guo, N. Psychogios, R. Mandal, S. M. Dunn, B. N. Ametaj and D. S. Wishart: The bovine ruminal fluid metabolome. *Metabolomics*, 9(2), 360-378 (2013)
24. R. Zhang, W. Zhu, L. Jiang and S. Mao: Comparative metabolome analysis of ruminal changes in Holstein dairy cows fed low-or high-concentrate diets. *Metabolomics*, 13(6), 74 (2017)
25. R. T. R. De Almeida, R. M. Do Prado, C. Porto, G. T. Dos Santos, S. A. Huws and E. J. Pilau: Exploring the rumen fluid metabolome using liquid chromatography-high-resolution mass spectrometry and Molecular Networking. *Scientific reports*, 8(1), 1-8 (2018)
26. D. Borges and F. d. A. Borges: Plants and their medicinal potential for controlling gastrointestinal nematodes in ruminants. *Nematoda*, 3, e92016 (2016)
27. F. Saleem, B. Ametaj, S. Bouatra, R. Mandal, Q. Zebeli, S. Dunn and D. Wishart: A metabolomics approach to uncover the effects of grain diets on rumen health in dairy cows. *Journal of Dairy Science*, 95(11), 6606-6623 (2012)
28. A. Checa, C. Bedia and J. Jaumot: Lipidomic data analysis: tutorial, practical guidelines and applications. *Analytica chimica acta*, 885, 1-16 (2015)
29. V. M. Artegoitia, A. P. Foote, R. M. Lewis and H. C. Freetly: Metabolomics Profile and Targeted Lipidomics in Multiple Tissues Associated with Feed Efficiency in Beef Steers. *ACS omega*, 4(2), 3973-3982 (2019)
30. D. Viglierchio and R. V. Schmitt: On the methodology of nematode extraction from field samples: Baermann funnel modifications. *Journal of nematology*, 15(3), 438 (1983)
31. S. Bisset, J. Knight and C. Bouchet: A multiplex PCR-based method to identify strongylid parasite larvae recovered from ovine faecal cultures and/or pasture samples. *Veterinary parasitology*, 200(1-2), 117-127 (2014)

32. N. Palevich, P. H. Maclean, A. Baten, R. W. Scott and D. M. Leathwick: The Genome Sequence of the Anthelmintic-Susceptible New Zealand *Haemonchus contortus*. *Genome biology and evolution*, 11(7), 1965-1970 (2019)
33. N. Palevich, P. Maclean, A. Baten, R. Scott and D. M. Leathwick: The complete mitochondrial genome of the New Zealand parasitic roundworm *Haemonchus contortus* (Trichostrongyloidea: Haemonchidae) field strain NZ_Hco_NP. *Mitochondrial DNA Part B*, 4(2), 2208-2210 (2019)
34. N. Palevich, P. H. Maclean, Y.-J. Choi and M. Mitreva: Characterization of the Complete Mitochondrial Genomes of Two Sibling Species of Parasitic Roundworms, *Haemonchus contortus* and *Teladorsagia circumcincta*. *Frontiers in Genetics*, 11(1066) (2020) doi:10.3389/fgene.2020.573395
35. N. Palevich, P. H. Maclean, M. Mitreva, R. Scott and D. Leathwick: The complete mitochondrial genome of the New Zealand parasitic roundworm *Teladorsagia circumcincta* (Trichostrongyloidea: Haemonchidae) field strain NZ_Teci_NP. *Mitochondrial DNA Part B*, 4(2), 2869-2871 (2019)
36. N. Palevich, W. J. Kelly, S. C. Leahy, E. Altermann, J. Rakonjac and G. T. Attwood: The complete genome sequence of the rumen bacterium *Butyrivibrio hungatei* MB2003. *Standards in Genomic Sciences*, 12(1), 72 (2017) doi:10.1186/s40793-017-0285-8
37. N. Palevich: Genome sequencing of rumen bacteria involved in lignocellulose digestion. In: *Institute of Molecular Biosciences*. Massey University, Palmerston North, New Zealand (2011)
38. N. Palevich: Comparative genomics of *Butyrivibrio* and *Pseudobutyrivibrio* from the rumen. In: *Institute of Fundamental Sciences*. Massey University, Palmerston North, New Zealand (2016)
39. N. Palevich, W. J. Kelly, S. Ganesh, J. Rakonjac and G. T. Attwood: *Butyrivibrio hungatei* MB2003 Competes Effectively for Soluble Sugars Released by *Butyrivibrio proteoclasticus* B316^{T} during Growth on Xylan or Pectin. *Applied and Environmental Microbiology*, 85(3), e02056-18 (2019) doi:10.1128/aem.02056-18
40. N. Palevich, W. J. Kelly, S. C. Leahy, S. Denman, E. Altermann, J. Rakonjac and G. T. Attwood: Comparative genomics of rumen *Butyrivibrio* spp. uncovers a continuum of polysaccharide-degrading capabilities. *Applied and environmental microbiology*, 86(1) (2019)

41. A. K. Subbaraj, Y. H. B. Kim, K. Fraser and M. M. Farouk: A hydrophilic interaction liquid chromatography–mass spectrometry (HILIC–MS) based metabolomics study on colour stability of ovine meat. *Meat science*, 117, 163-172 (2016)

42. M. Su, A. K. Subbaraj, K. Fraser, X. Qi, H. Jia, W. Chen, M. Gomes Reis, M. Agnew, L. Day and N. C. Roy: Lipidomics of Brain Tissues in Rats Fed Human Milk from Chinese Mothers or Commercial Infant Formula. *Metabolites*, 9(11), 253 (2019)

43. A. K. Subbaraj, J. Huege, K. Fraser, M. Cao, S. Rasmussen, M. Faville, S. J. Harrison and C. S. Jones: A large-scale metabolomics study to harness chemical diversity and explore biochemical mechanisms in ryegrass. *Communications biology*, 2(1), 1-17 (2019)

44. J. Godzien, V. Alonso-Herranz, C. Barbas and E. G. Armitage: Controlling the quality of metabolomics data: new strategies to get the best out of the QC sample. *Metabolomics*, 11, 518-528 (2015)

45. K. Fraser, G. A. Lane, D. E. Otter, Y. Hemar, S.-Y. Quek, S. J. Harrison and S. Rasmussen: Analysis of metabolic markers of tea origin by UHPLC and high resolution mass spectrometry. *Food Research International*, 53(2), 827-835 (2013)

46. K. Fraser, S. J. Harrison, G. A. Lane, D. E. Otter, Y. Hemar, S.-Y. Quek and S. Rasmussen: Non-targeted analysis of tea by hydrophilic interaction liquid chromatography and high resolution mass spectrometry. *Food chemistry*, 134(3), 1616-1623 (2012)

47. E. M. Forsberg, T. Huan, D. Rinehart, H. P. Benton, B. Warth, B. Hilmers and G. Siuzdak: Data processing, multi-omic pathway mapping, and metabolite activity analysis using XCMS Online. *Nature protocols*, 13(4), 633 (2018)

48. J. Xia, I. V. Sinelnikov, B. Han and D. S. Wishart: MetaboAnalyst 3.0—making metabolomics more meaningful. *Nucleic acids research*, 43(W1), W251-W257 (2015)

49. C. A. Smith, E. J. Want, G. O'Maille, R. Abagyan and G. Siuzdak: XCMS: processing mass spectrometry data for metabolite profiling using nonlinear peak alignment, matching, and identification. *Analytical chemistry*, 78(3), 779-787 (2006)

50. W. B. Dunn, I. D. Wilson, A. W. Nicholls and D. Broadhurst: The importance of experimental design and QC samples in large-scale and MS-driven untargeted metabolomic studies of humans (2012)

51. H. M. Parsons, D. R. Ekman, T. W. Collette and M. R. Viant: Spectral relative standard deviation: a practical benchmark in metabolomics. *Analyst*, 134(3), 478-485 (2009)
52. M. Cao, K. Fraser, C. Jones, A. Stewart, T. Lyons, M. Faville and B. Barrett: Untargeted metabotyping Lolium perenne reveals population-level variation in plant flavonoids and alkaloids. *Frontiers in plant science*, 8, 133 (2017)
53. C. Guijas, J. R. Montenegro-Burke, X. Domingo-Almenara, A. Palermo, B. Warth, G. Hermann, G. Koellensperger, T. Huan, W. Uritboonthai and A. E. Aisporna: METLIN: a technology platform for identifying knowns and unknowns. *Analytical chemistry*, 90(5), 3156-3164 (2018)
54. D. S. Wishart, Y. D. Feunang, A. Marcu, A. C. Guo, K. Liang, R. Vázquez-Fresno, T. Sajed, D. Johnson, C. Li and N. Karu: HMDB 4.0: the human metabolome database for 2018. *Nucleic acids research*, 46(D1), D608-D617 (2018)
55. E. Fahy, M. Sud, D. Cotter and S. Subramaniam: LIPID MAPS online tools for lipid research. *Nucleic acids research*, 35(suppl_2), W606-W612 (2007)
56. B. Wheeler, M. Torchiano and M. Torchiano: Package 'lmPerm'. R package version, 2.1. 0. In, (2016)
57. Y. Benjamini and Y. Hochberg: Controlling the false discovery rate: a practical and powerful approach to multiple testing. *Journal of the Royal statistical society: series B (Methodological)*, 57(1), 289-300 (1995)
58. A. Zeileis, M. A. Wiel, K. Hornik and T. Hothorn: Implementing a class of permutation tests: the coin package. *Journal of statistical software*, 28(8), 1-23 (2008)
59. S. Li, Y. Park, S. Duraisingham, F. H. Strobel, N. Khan, Q. A. Soltow, D. P. Jones and B. Pulendran: Predicting network activity from high throughput metabolomics. *PLoS Comput Biol*, 9(7), e1003123 (2013)
60. R. Ihaka and R. Gentleman: R: a language for data analysis and graphics. *Journal of computational and graphical statistics*, 5(3), 299-314 (1996)
61. G. K. Smyth, M. Ritchie, N. Thorne and J. Wettenhall: LIMMA: linear models for microarray data. In Bioinformatics and Computational Biology Solutions Using R and Bioconductor. Statistics for Biology and Health (2005)

62. M. Cao, K. Fraser, J. Huege, T. Featonby, S. Rasmussen and C. Jones: Predicting retention time in hydrophilic interaction liquid chromatography mass spectrometry and its use for peak annotation in metabolomics. *Metabolomics*, 11(3), 696-706 (2015) doi:10.1007/s11306-014-0727-x
63. L. R. Campbell and R. Gaugler: Mechanisms for exsheathment of entomopathogenic nematodes. *International journal for parasitology*, 21(2), 219-224 (1991)
64. G. Lapage: The second ecdysis of infective nematode larvae. *Parasitology*, 27(2), 186-206 (1935)
65. J. Van Wyk: Viability of nematode larvae after exsheathment with sodium hypochlorite. *Parasitology today (Personal ed.)*, 14(12), 474 (1998)
66. G. Ma, R. B. Gasser, T. Wang, P. K. Korhonen and N. D. Young: Toward integrative 'omics of the barber's pole worm and related parasitic nematodes. *Infection, Genetics and Evolution*, 104500 (2020)
67. J. Barrett: Biochemistry of parasitic helminths. MacMillan Publishers Ltd., (1981)
68. J. Kapur and M. Sood: Biochemistry of *Haemonchus*-a review. *Angewandte Parasitologie*, 28(4), 211 (1987)
69. H. Van den Bossche, O. Vanparijs and D. Thienpont: Studies on the carbohydrate metabolism of third-stage *Haemonchus contortus* larvae. *Life sciences*, 8(20), 1047-1054 (1969)
70. M. G. Vander Heiden, L. C. Cantley and C. B. Thompson: Understanding the Warburg effect: the metabolic requirements of cell proliferation. *science*, 324(5930), 1029-1033 (2009)
71. N. Palevich, P. H. Maclean, W. J. Kelly, S. C. Leahy, J. Rakonjac and G. T. Attwood: Complete Genome Sequence of the Polysaccharide-Degrading Rumen Bacterium Pseudobutyrivibrio xylanivorans MA3014 Reveals an Incomplete Glycolytic Pathway. *Genome Biology and Evolution*, 12(9), 1566-1572 (2020) doi:10.1093/gbe/evaa165
72. R. E. Hungate: The rumen microbial ecosystem. In: *Annual Review of Ecology and Systematics*. Ed R. F. Johnston, P. W. Frank&C. D. Michener. Annual Reviews, California, USA (1975)
73. A. Harder: The biochemistry of *Haemonchus contortus* and other parasitic nematodes. In: *Advances in parasitology*. Elsevier, (2016)

74. J. Mansfeld, N. Urban, S. Priebe, M. Groth, C. Frahm, N. Hartmann, J. Gebauer, M. Ravichandran, A. Dommaschk and S. Schmeisser: Branched-chain amino acid catabolism is a conserved regulator of physiological ageing. *Nature communications*, 6(1), 1-12 (2015)

75. S. Fuchs, J. G. Bundy, S. K. Davies, J. M. Viney, J. S. Swire and A. M. Leroi: A metabolic signature of long life in *Caenorhabditis elegans*. *BMC biology*, 8(1), 1-12 (2010)

76. J. Walker and J. Barrett: Parasite sulphur amino acid metabolism. *International Journal for Parasitology*, 27(8), 883-897 (1997) doi:https://doi.org/10.1016/S0020-7519(97)00039-8

77. T. Wang, S. Nie, G. Ma, P. K. Korhonen, A. V. Koehler, C.-S. Ang, G. E. Reid, N. A. Williamson and R. B. Gasser: The developmental lipidome of *Haemonchus contortus*. *International journal for parasitology*, 48(12), 887-895 (2018)

78. M. J. Wargo, B. S. Szwergold and D. A. Hogan: Identification of two gene clusters and a transcriptional regulator required for *Pseudomonas aeruginosa* glycine betaine catabolism. *Journal of bacteriology*, 190(8), 2690-2699 (2008)

79. S. Umair, C. Ria, J. Knight, R. Bland and H. Simpson: Sarcosine metabolism in *Haemonchus contortus* and *Teladorsagia circumcincta*. *Experimental parasitology*, 134(1), 1-6 (2013)

80. M. Wyss and R. Kaddurah-Daouk: Creatine and creatinine metabolism. *Physiological reviews* (2000)

81. E. Platzer, S. Thompson, D. Borchardt and H. Gamble: High energy phosphate metabolites observed by NMR in infective larvae of *Haemonchus contortus*. *The Journal of parasitology*, 434-438 (1995)

82. S. Umair, J. Knight, R. Bland and H. Simpson: Molecular and biochemical characterisation of arginine kinases in *Haemonchus contortus* and *Teladorsagia circumcincta*. *Experimental parasitology*, 134(3), 362-367 (2013)

83. P. Murray, S. A. L. Hayward, G. G. Govan, A. Y. Gracey and A. R. Cossins: An explicit test of the phospholipid saturation hypothesis of acquired cold tolerance in *Caenorhabditis elegans*. *Proceedings of the National Academy of Sciences*, 104(13), 5489-5494 (2007) doi:10.1073/pnas.0609590104

84. Dengke K. Ma, Z. Li, Alice Y. Lu, F. Sun, S. Chen, M. Rothe, R. Menzel, F. Sun and H. R. Horvitz: Acyl-CoA Dehydrogenase Drives Heat Adaptation by Sequestering Fatty Acids. *Cell*, 161(5), 1152-1163 (2015) doi:https://doi.org/10.1016/j.cell.2015.04.026

85. X. Bellés, D. Martín and M.-D. Piulachs: The mevalonate pathway and the synthesis of juvenile hormone in insects. *Annu. Rev. Entomol.*, 50, 181-199 (2005)
86. W. Rogers: Juvenile and moulting hormones from nematodes. *Parasitology*, 67(1), 105-113 (1973)
87. K. Davey: Molting in a parasitic nematode, Phocanema decipiens—VI The mode of action of insect juvenile hormone and farnesyl methyl ether. *International journal for parasitology*, 1(1), 61-66 (1971)
88. S. Höss and L. Weltje: Endocrine disruption in nematodes: effects and mechanisms. *Ecotoxicology*, 16(1), 15-28 (2007)

Figure Legends

Figure 1. Overview of the experimental design and multimodal metabolomics workflow. **(A)** New Zealand pasture-fed sheep used for this study. **(B)** Dialyzed rumen fluid (DRF) fractions were obtained under anaerobic rumen conditions (39°C and CO_2) using dialysis systems at three molecular weight cut-offs (MWCOs), 20 kDa, 8-10 kDa and 100 Da. **(C)** *In vitro* testing using a closed anaerobic system (39°C and CO_2) of DRF fractions and control treatments of filtered RF, saline (PBS) and distilled water (dH_2O) on third-stage larval (L3) exsheathment in *H. contortus*. **(D)** Exsheathment activity of *H. contortus* L3's in various DRF fractions and control treatments after 12 h reactivation in a closed anaerobic system (39°C and CO_2). There was no exsheathment activity observed in the absence of 39°C or CO_2 for any treatment conditions. **(E)** Schematic of a multimodal metabolomics workflow and statistical analyses used to process data integrated from multiple analytical approaches and pathway mapping.

Figure 2. Multigroup DRF fraction metabolic profiles for all metabolomics streams. **(A-F)** Scores plots for Partial least squares-discriminant analysis (PLS-DA) for the different DRF fraction metabolic profiles identified using HILIC positive **(A)** and negative **(B)** streams, C18 positive **(C)** and negative **(D)** streams, LIPID positive **(E)** and negative **(F)** streams. A five-component modeling was performed by PLS-DA using MetaboAnalyst 4.0 program. Ovals show 95% confidence interval for each DRF fraction. Each MWCO or DRF fraction was colored to represent 20 kDa (green), 8-10 kDa (purple), 100 Da (red) and PBS control (blue). The scatter plots shown represent plots with the 2 components having the greatest variations.

Observations that are similar will fall close to each other displaying a clustering-like pattern. One data point represents one biological replicate.

Figure 3. Unique and mutual metabolites identified across all metabolomics streams. Venn diagrams compiling the Polar (HILIC-MS), semi-polar (C18-MS) and non-polar compounds (LIPID using a non-targeted technique) molecular features determined from all DRF fractions (20 kDa, 8-10 kDa, 100 Da MWCOs) and PBS control, for the negative **(A)** and positive **(B)** streams. Extracts were analyzed using ultra-high-performance liquid chromatography coupled to a high-resolution mass spectrometer (UHPLC-MS). UpsetR barchart analysis **(C)** showing the presence and numbers of quantified molecular features determined for different metabolomics streams (i.e. HILIC$^{+/-}$ (orange), C18$^{+/-}$ (purple) and LIPID$^{+/-}$ (blue). Connected dots display shared molecular features between or among metabolomics streams, and the total number of features in a particular metabolomics stream is shown in the set size. Colored connected dots indicate the molecular features identified in both the negative and positive extractions of a metabolomics stream.

Figure 4. Diversity and grouping of metabolites identified for each metabolomics stream. Boxplots of top peak intensities of example compounds **(A)** and nucleic acids **(B)** identified with high confidence via the non-targeted C18 and HILIC methods. **(C)** Cladogram depicting the three group classifications of all LIPID species. **(D)** Boxplots of peak intensities of example lipid compounds identified by the non-targeted lipidomics method. Each MWCO or DRF fraction is represented as 20 kDa (DRF1), 8-10 kDa (DRF2), 100 Da (DRF3) and PBS control treatments.

Figure S1. Extraction protocol treatment of DRF samples in preparation for all metabolomics streams.

Figure S2. The metabolomics workflow used to illustrate the series of steps from raw data collection through to compound identification and pathway analysis via database searching.

Figure S3. Example extracted ion chromatogram (XIC) plots. **(A)** The overall XIC plot of of amino acid standards in C18 (blue) and Hillic (red) columns. **(B)** The smoothed XIC of Methionine (M+H, computed mass *m/z* 150.0589) showing the retention time of 1.11 min in C18 and 10.64 min in HILIC.

Figure S4. Multivariate analysis of DRF fraction profiles for the LIPID stream. **(A)** Principal component analysis (PCA) based on 28,664 LP peaks. Scores plots for Partial least squares-discriminant analysis (PLS-DA) for the different DRF fraction metabolic profiles of the 28,664 LP **(B)** and 13,629 LN **(C)** peaks identified

using the LIPID streams. Ovals show 95% confidence interval for each DRF fraction. Each MWCO or DRF fraction is colored to represent 20 kDa (DRF1), 8-10 kDa (DRF2), 100 Da (DRF3) and PBS control (blue). The scatter plots shown represent plots with the 2 components having the greatest variations. Observations that are similar will fall close to each other displaying a clustering-like pattern. One data point represents one biological replicate.

Figure S5. Hierarchical Clustering heatmaps showing the top 50 metabolites identified across all metabolomics streams. **(A-F)** Hierarchical clustering was performed for the different DRF fraction metabolic profiles identified using HILIC positive **(A)** and negative **(B)**, C18 positive **(C)** and negative **(D)**, LIPID positive **(E)** and negative **(F)** streams. Comparisons considered the top fifty Benjamini-Hochberg FDR corrected t-test p value (<0.05) passing metabolite features with clustering performing using Metaboanalyst 4.0. Horizontal axis is all the samples analyzed in the study and vertical axis denotes METLIN accessions for top 50 metabolite features. Full-length descriptions and feature names are available in Supplementary Table S4. On top of the heatmap are the MWCOs or DRF fractions to represent 20 kDa (green), 8-10 kDa (dark blue), 100 Da (red) and PBS control (light blue) colored squares. Dendrogram for samples is shown on top of the heatmap and features' dendrogram on left side of the heatmap. Dark blue to dark red color gradient denotes lower to higher expression.

Figure S6. Example of correlated CP peaks among samples. The orange colored group of peaks are readily found high in one biological treatment (i.e. PBS).

Figure S7. Boxplot showing the LP614.572_8.62 lipid species based on the normalized peak heights and fragmentation data.

Table Legends

Table 1. Summary of compounds identified across all metabolomics streams (HILIC, C18 and LIPID) and DRF fractions.

Table S1. Normalized peak tables for HILIC species in all DRF fractions in both positive (HP) and negative (HN) ionization modes. The *m/z* mass-to-charge ratio of the features used for identification; RT denotes retention time in minutes.

Table S2. Normalized peak tables for C18 species in all DRF fractions in both positive (CP) and negative (CN) ionization modes. The *m/z* mass-to-charge ratio of the features used for identification; RT denotes retention time in minutes.

Table S3. Normalized peak tables for lipid species in all DRF fractions in both positive (LP) and negative (LN) ionization modes. The *m/z* mass-to-charge ratio of the features used for identification; RT denotes retention time in minutes.

Table 1. Summary of compounds identified across all metabolomics streams (HILIC, C18 and LIPID) and DRF fractions.

Class	Stream	Species name	Monoisotopic peak (*m/z*_rt)	Isotopic peak (*m/z*_rt)	Ion type	Note
C18 and HILIC						
Amino acids	CP	Methionine		150.0584_1.08	$[M+H]^+$	**Group 1**
	HP			150.0583_10.56	$[M+H]^+$	
	CP	Leucine		132.1019_1.85	$[M+H]^+$	
	HP			132.1021_9.85	$[M+H]^+$	
	HP	Alanine		90.0554_12.54	$[M+H]^+$	
	HP	Phenylalanine		166.0862_9.81	$[M+H]^+$	
	HN			164.071_9.84	$[M+H]^-$	
Purine or pyrimidine	CP	Xanthine		153.0408_1.37	$[M+H]^+$	
	CP	Hypoxanthine		137.0459_1.17	$[M+H]^+$	
	HP			137.0456_8.25	$[M+H]^+$	
	HN			135.0305_8.38	$[M+H]^-$	
Nucleic acids	HP	Adenine		136.0617_8.54	$[M+H]^+$	**Group 2**
	HP	Guanine		152.0566_10.18	$[M+H]^+$	
	HP	Cytosine		112.0508_10.72	$[M+H]^+$	
	HP	Adenosine		268.1038_8.06	$[M+H]^+$	
Plant secondary metabolites	CP	Indole carbinol		148.0757_5.54	$[M+H]^+$	
	CP	Hydroxy dimethoxy flavone		299.0915_5.17	$[M+H]^+$	
	CP	Phytoalexin		237.185_6.94	$[M+H]^+$	**Group 3**
	HN	Lactic acid		89.0235_2.73	$[M+H]^-$	**Group 1 and 3**
	HN	Succinic acid		117.0186_4.00	$[M+H]^-$	
LIPIDS						
LPG	LP	C16:0	485.2905_2.41	486.2931_2.41	$[M+H]^+$	**Group 3**
	LP		502.3172_2.41	503.3204_2.41	$[M+NH_4]^+$	
	LP	C18:0	530.3487_2.41	531.352_2.41	$[M+NH_4]^+$	
	LP	C18:3	507.2725_2.41		$[M+NH_4]^+$	
	LP	C20:0	558.381_2.41	559.3838_2.41	$[M+NH_4]^+$	
	LP	C21:0	572.3964_2.41		$[M+NH_4]^+$	
	LP	C22:0	586.4116_2.41	587.4147_2.41	$[M+NH_4]^+$	
Sterol	LN	Campesterol ester	705.5767_8.36	706.5802_8.36	$[M+FA-H]^-$	
	LN			707.5833_8.36		
DG	LP	C37:1	654.6034_8.61	655.6066_8.61	$[M+NH_4]^+$	
	LP	C16:0 C18:0	614.572_8.62	614.598_8.62	$[M+NH_4]^+$	**Group 1**
TG*	LP	C48:1	822.755_11.37	823.758_11.38	$[M+NH_4]^+$	
	LP	C54:4	883.7739_12.2	884.7785_12.2	$[M+H]^+$	
	LP	C52:1	878.8175_12.2	879.8205_12.2	$[M+NH_4]^+$	
PC	LP	C32:5	724.4897_7.53	725.4929_7.53	$[M+H]^+$	**Group 2**
	LP	C34:5	752.5202_7.53	753.5237_7.53	$[M+H]^+$	
	LP	C35:5	766.5358_7.53	767.5387_7.53	$[M+H]^+$	
	LP	OHOHA-PC	679.4316_7.53	680.4357_7.53	$[M+NH_4]^+$	

Compounds were identified by matching with a local library of authentic standards, public domain mass spectral databases and analytical stream. All metabolite identifications are classed with Level 2 confidence. *A few other TG species may be eluting around 12 min, but without the support of isotopic peaks. For example, LP852.7977_11.96, LP862.7878_11.78, LP934.8795_11.96 may be annotated as TG 50:0, TG 51:2 and TG 56:1, respectively, it is $[M+NH4]^+$. Abbreviations: LPG, lysophosphatidylglycerol; DG, diglyceride; PC, phosphatidylcholine; TG, triglyceride. C16:0, C18:0, C18:3, etc. refer to fatty acids with their respective number of carbon atoms and double bonds

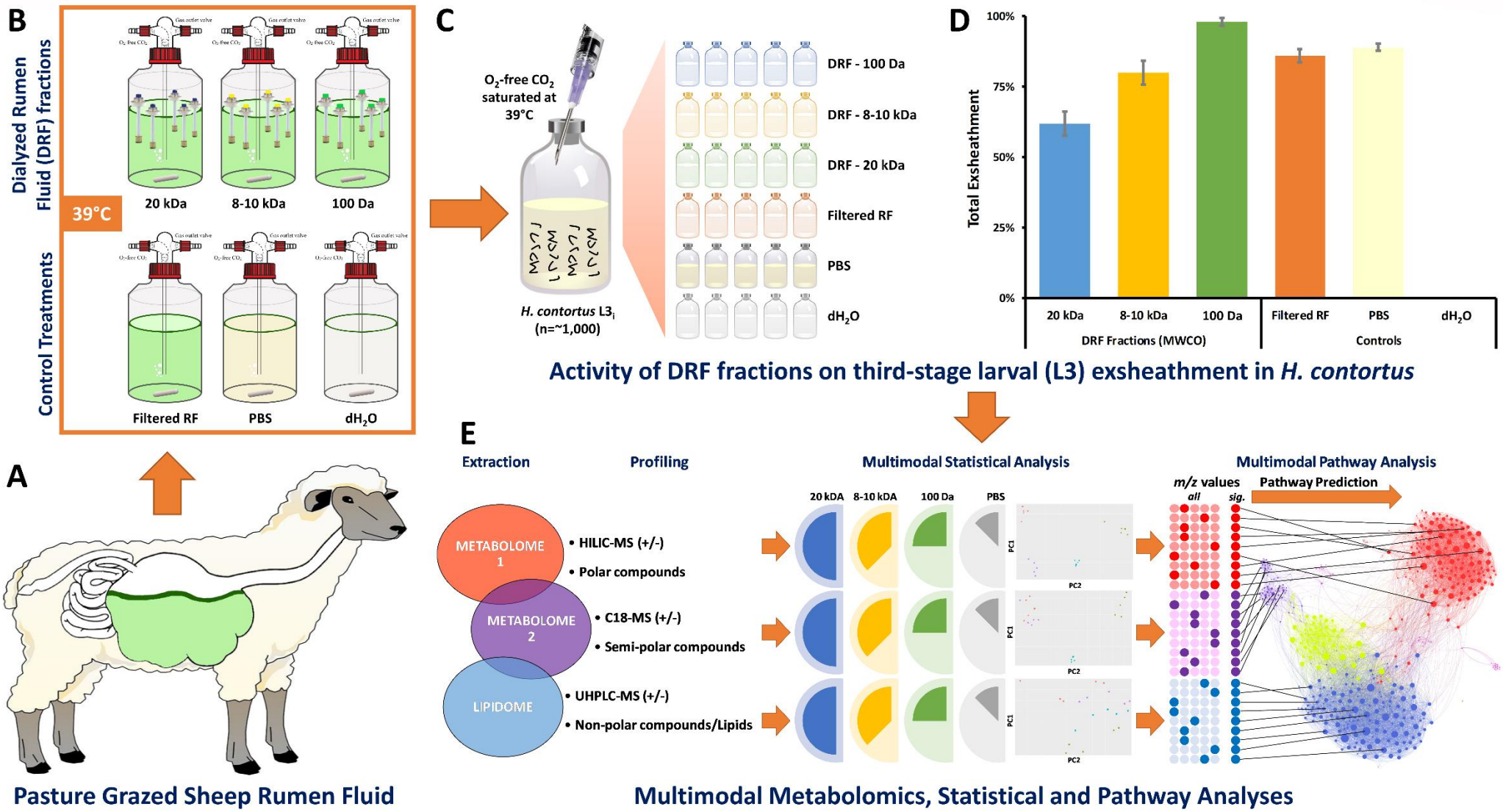
B
Dialyzed Rumen Fluid (DRF) fractions
39°C
20 kDa
8-10 kDa
100 Da
Control Treatments
Filtered RF
PBS
dH2O
C
O2-free CO2 saturated at 39°C
H. contortus L3i (n=~1,000)
DRF - 100 Da
DRF - 8-10 kDa
DRF - 20 kDa
Filtered RF
PBS
dH2O
D
Total Exsheathment
100%
75%
50%
25%
0%
20 kDa
8-10 kDa
100 Da
Filtered RF
PBS
dH2O
DRF Fractions (MWCO)
Controls
Activity of DRF fractions on third-stage larval (L3) exsheathment in H. contortus
A
Pasture Grazed Sheep Rumen Fluid
E
Extraction
Profiling
Multimodal Statistical Analysis
Multimodal Pathway Analysis
m/z values
all
sig.
Pathway Prediction
20 kDA
8-10 kDA
100 Da
PBS
METABOLOME 1
METABOLOME 2
LIPIDOME
• HILIC-MS (+/-)
• Polar compounds
• C18-MS (+/-)
• Semi-polar compounds
• UHPLC-MS (+/-)
• Non-polar compounds/Lipids
PC1
PC2
Multimodal Metabolomics, Statistical and Pathway Analyses

Figure 1

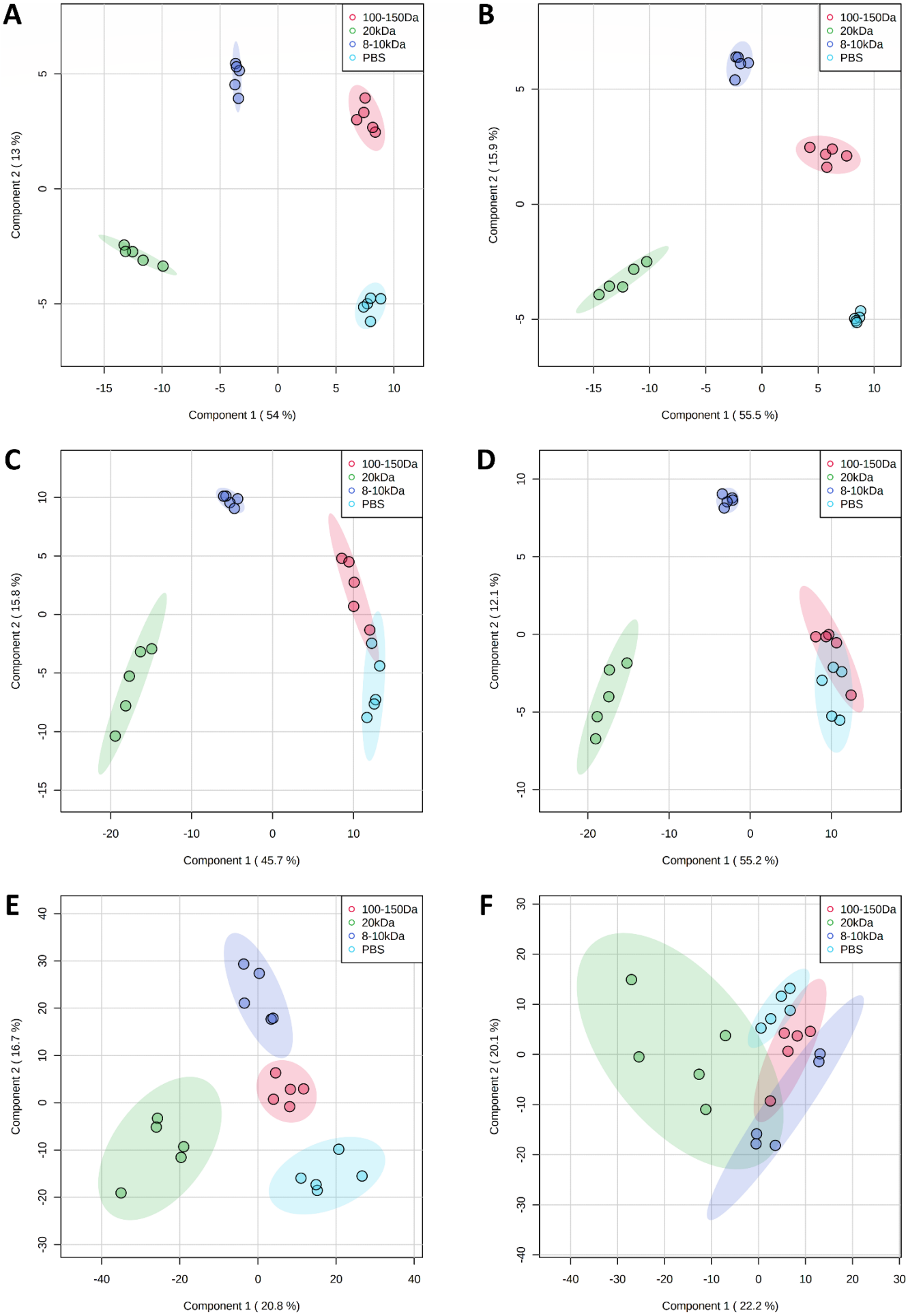
A
100-150Da
20kDa
8-10kDa
PBS
Component 2 (13 %)
Component 1 (54 %)
B
Component 2 (15.9 %)
Component 1 (55.5 %)
C
Component 2 (15.8 %)
Component 1 (45.7 %)
D
Component 2 (12.1 %)
Component 1 (55.2 %)
E
Component 2 (16.7 %)
Component 1 (20.8 %)
F
Component 2 (20.1 %)
Component 1 (22.2 %)

Figure 2

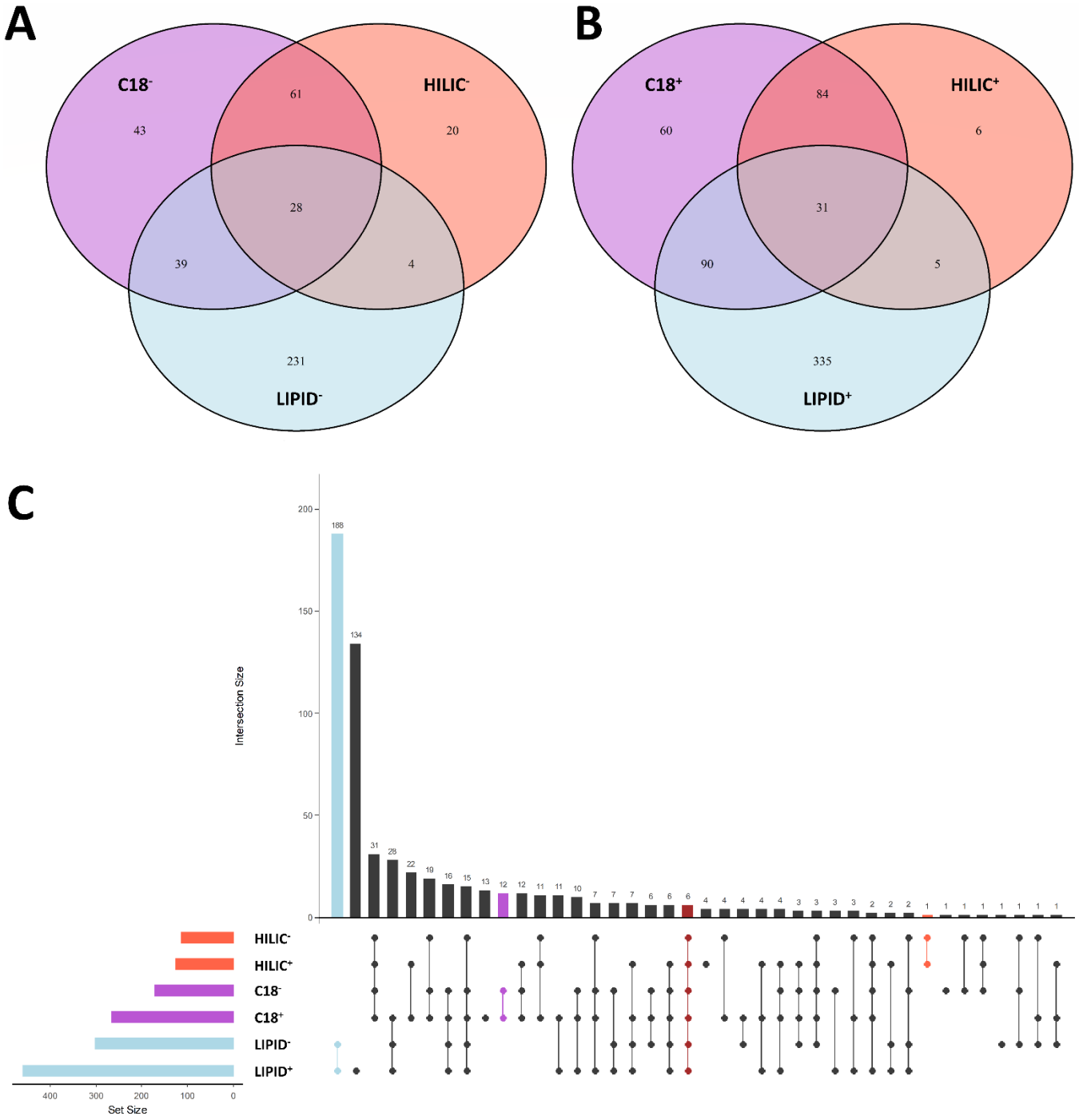
A
C18-
HILIC-
LIPID-
43
61
20
28
39
4
231
B
C18+
HILIC+
LIPID+
60
84
6
31
90
5
335
C
Intersection Size
Set Size
HILIC-
HILIC+
C18-
C18+
LIPID-
LIPID+

Figure 3

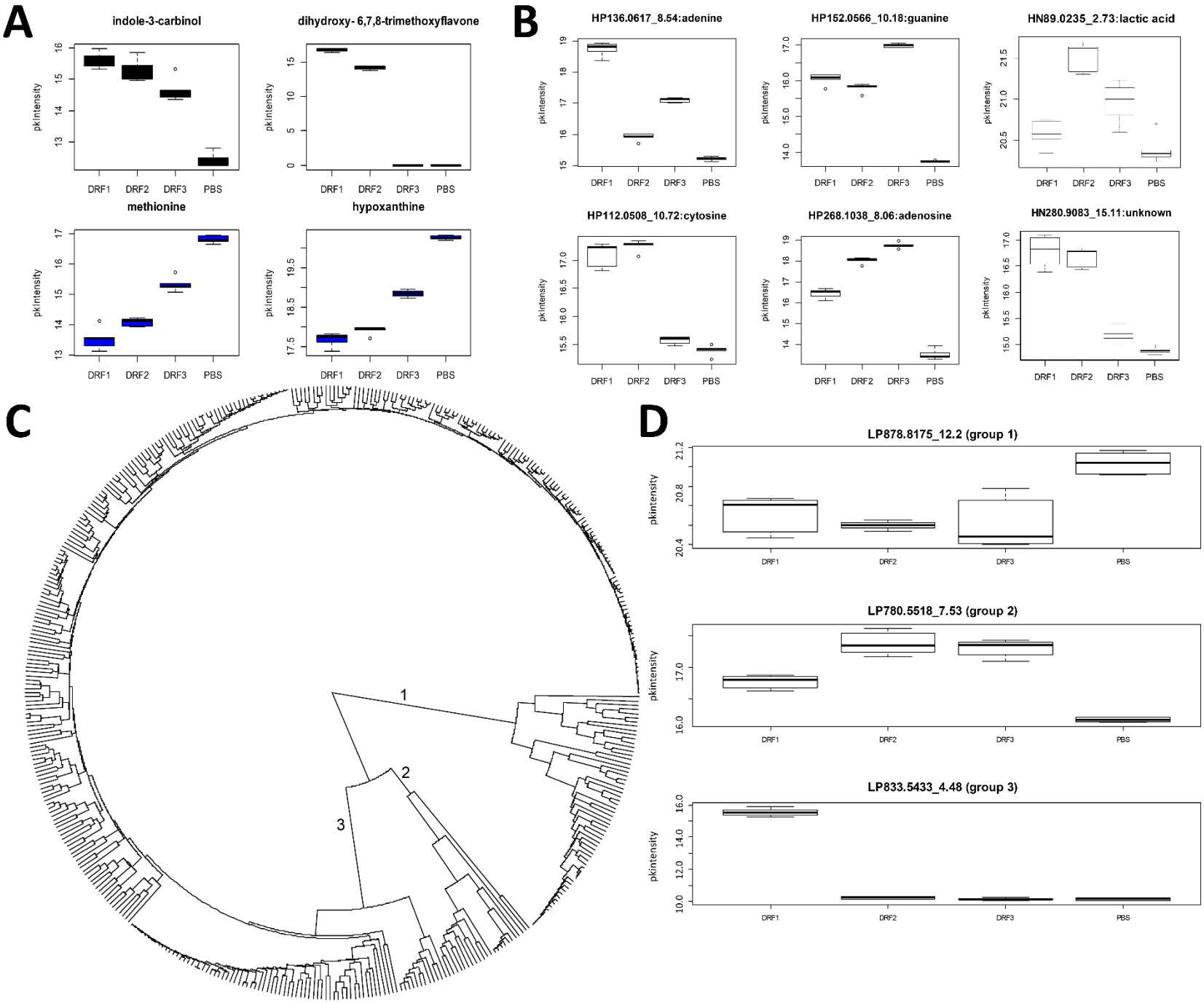
A
indole-3-carbinol
dihydroxy- 6,7,8-trimethoxyflavone
methionine
hypoxanthine
pkIntensity
DRF1
DRF2
DRF3
PBS
B
HP136.0617_8.54:adenine
HP152.0566_10.18:guanine
HN89.0235_2.73:lactic acid
HP112.0508_10.72:cytosine
HP268.1038_8.06:adenosine
HN280.9083_15.11:unknown
C
1
2
3
D
LP878.8175_12.2 (group 1)
LP780.5518_7.53 (group 2)
LP833.5433_4.48 (group 3)

941

Figure 4